Journal of Applied Polymer Science

Effect of electric field on polymer/clay nanocomposites depending on the affinities between the polymer and clay

Hyun Geun Ock, Kyung Hyun Ahn, Seung Jong Lee
School of Chemical and Biological Engineering, Seoul National University, Seoul, 08826, Korea
Correspondence to: K. H. Ahn (E-mail: ahnnet@snu.ac.kr)

ABSTRACT: Applying an electric field is an efficient way to fabricate polymer/clay nanocomposites. It helps to achieve a good dispersion of nanoclays which improves the performance of the polymeric system. In this study, the effect of an alternating current (A.C.) electric field was investigated on clay exfoliation with various combinations of polymer/clay nanocomposites. Three different types of organoclays (Cloisite 10A, 20A, 30B) were introduced in polypropylene (PP) and poly(lactic acid) (PLA) matrices. Their rheological properties showed that the A.C. electric field was effective in enhancing the dispersion of organoclays in both the PP/clay and PLA/clay composites. The efficiency of the A.C. field varied depending on the combination of polymer and clay nanoparticles. In the case of PP, the best combination was PP/C20A followed by PP/C10A and PP/C30B. In contrast, PLA/clay showed an opposite trend. This difference arises from the different affinities between the polymers and the functional groups of the clays. The Hansen solubility parameter was introduced to quantify the affinities between the polymer and clay. The electric field was more effective for polymer/clay combinations that had less difference in the Hansen solubility parameter. © 2016 Wiley Periodicals, Inc. J. Appl. Polym. Sci. **2016**, *133*, 43582.

KEYWORDS: clay; composites; rheology

Received 12 December 2015; accepted 27 February 2016
DOI: 10.1002/app.43582

INTRODUCTION

Physical properties of polymer can be improved by adding small amount of nanoparticles. [1–4] This hybrid material system is called polymer nanocomposites. Especially, clay is one of the most widely used nanoparticles to fabricate polymer nanocomposites due to its large surface area and high aspect ratio. The performance of polymers such as mechanical properties, heat resistance, flame retardancy, gas barrier properties, and biodegradability could be enhanced with relatively small amount of clay content compared with conventional micron-sized fillers.[5–12] In order to obtain distinct characteristics of nanoclay in polymer/clay nanocomposites, it is essential to delaminate stacks of clay layers, which is called clay exfoliation.[13] There have been many studies on clay exfoliation in polymer melts which can be classified into chemical and physical methods. The chemical methods include solution casting, *in situ* polymerization and the use of compatibilizers.[14,15] On the other hand, the physical approaches include applying external fields such as electric field, magnetic field, and ultrasound application.[16–18] Especially, applying the electric field is unique in fabricating polymer/clay nanocomposites. The effect of alternating current (A.C.) electric field for polypropylene (PP)/clay nanocomposite was firstly reported in 2003.[1] It was found that an A.C. field caused exfoliation, while a D.C. field induced orientation of the clay particles.[2] Also, Kim *et al.* confirmed that the number of bound ions on the clay surface decreased with the application of an electric field, using dielectric analysis. The degree of exfoliation of clay was enhanced due to the imbalance between the van der Waals attraction and the electrostatic repulsion which was originated from the dissociation of the bound ions from the clay surfaces.[3]

In previous studies, only one polymer/clay nanocomposite system (PP/Cloisite 20A) was used as a model system.[1–4] The interaction between polymers and clays on the structural change under the electric field has not been probed yet. In this study, several polymer/clay combinations were introduced to examine their structural development according to the affinities between the polymers and clays under an electric field. PP, a non-polar polymer, and poly(lactic acid) (PLA), a polar polymer, were used as base polymers. Three types of clays with different surfactants (Cloisite 10A, Cloisite 20A, Cloisite 30B) were melt mixed with both PP and PLA. The effect of electric field on the structural development of the polymer/clay nanocomposites according to various polymer/clay combinations was investigated through morphological observations as well as rheological analysis. The effect of the affinities between the polymers and

Table I. Material Information

Substance	Trademark	Characteristics	Supplier
PP	HP740T	Melt Flow rate (230 °C/2.16 kg) = 6.0 g/min	PolyMirae Co. Ltd
PLA	4032D	Melt Flow rate (200 °C/2.16kg) = 1.0 g/min	Nature Works Co. Ltd.
C10A	Cloisite®10A	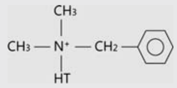 HT: Hydrogenated Tallow (~65% C18; ~30% C16; ~5% C14)	Southern Clay Products, Inc.
C20A	Cloisite®20A	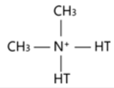	Southern Clay Products, Inc.
C30B	Cloisite®30B	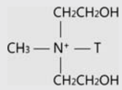 T: Tallow (~65% C18; ~30% C16; ~5% C14)	Southern Clay Products, Inc.

clays on the efficiency of the electric field in clay dispersion was also examined.

EXPERIMENTAL

Materials and Sample Preparation

The PP (HP740T) used in this study was supplied by PolyMirae Co. LTD. The PLA (4032D) was provided by Natureworks Co. LTD. Three different commercial grades of organoclays, Cloisite 10A, Cloisite 20A, Cloisite 30B, were obtained from Southern Clay Product. The clay content was fixed to 5 wt %. All the samples were used after drying in a vacuum oven for 12 h at 80 °CC. The nanocomposites were prepared by melt compounding using an intensive mixer (Rheomix 600 & Rheocord 90, Haake) at 100 rpm for 10 min at different temperature, 190 °C for PP and 210 °C for PLA in order to match the applied shear stress at a given mixing rpm. Information about the materials used in the study is presented in Table I, and the notations of each polymer/clay nanocomposites are listed in Table II.

Electric Field Activation

Prior to measuring the rheological properties, a specimen with a thickness of 1 mm and a diameter of 25 mm was prepared by compression molding for 6 min using a hot press (Carver, CH4386) at the same temperature with melt compounding. As shown in Figure 1, the fixture of a conventional rheometer (RMS-800, Rheometrics) was modified to directly apply an A.C. field during the dynamic time sweep test.[1–4] The electric field was applied using a function generator (AFG 310, Tektronix) and a high-voltage amplifier (677B, Trek). The A.C. field was applied for 20 min at a fixed A.C. frequency of 60 Hz with various field strengths (325, 550, 775, and 1000 V/mm) at 20 °C lower temperature than compounding condition depending on the polymeric systems. A dynamic time sweep test was conducted at a fixed angular frequency ($\omega = 1$ rad/s) during applying the A.C. electric field. In order to examine the structural change of nanocomposites under the electric field, the normalized G' growth, $[(G'(t) - G'_0)/G'_0]$, was introduced. Here, G'_0 is G' at $t = 0$, $G'(t)$ is G' at time t, and G'_{infinity} is G' at $t = 1200$ s.

Table II. Sample Notation (the Numbers in Parentheses are the Compositions)

Polymer	Organoclay	Nanocomposite
	C10A (5%)	PP10A
PP (95%)	C20A (5%)	PP20A
	C30B (5%)	PP30B
	C10A (5%)	PL10A
PLA (95%)	C20A (5%)	PL20A
	C30B (5%)	PL30B

Characterization

A dynamic frequency sweep test before and after applying the electric field was performed at a frequency range from 0.1 to 100 rad/s within a linear strain regime in order to observe the structural development of the nanocomposites. The rheological property of PP/clay was measured at 170 °C, while that of PLA/clay was measured at 190 °C. The degree of clay dispersion after

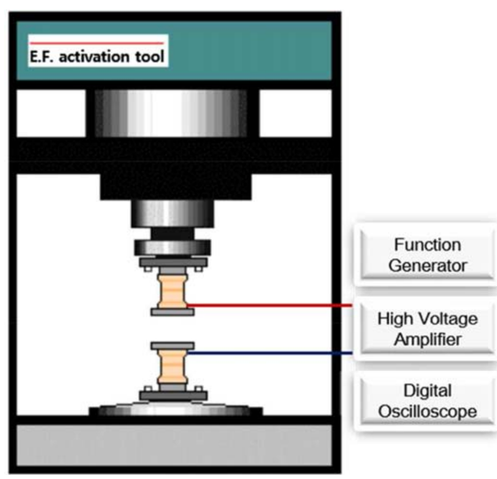

Figure 1. Schematic representation of electric field activation tool in a conventional rheometer. [Color figure can be viewed in the online issue, which is available at wileyonlinelibrary.com.]

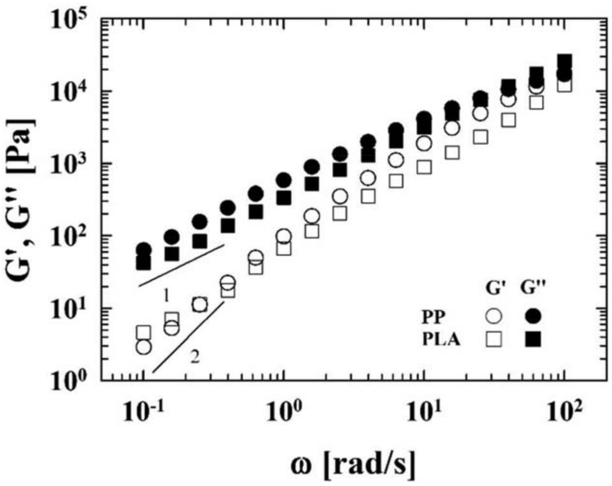

Figure 2. G' and G'' as a function of the angular frequency for neat PP at 170 °C and neat PLA at 190 °C.

the application of an electric field was confirmed by Transmission Electron Microscopy (JEOL 2100F at an acceleration voltage of 200 kV). The electric field treated samples were cut by cryo-ultramicrotomy for TEM observation.

RESULTS AND DISCUSSION

Effect of Electric Field on Clay Dispersion

The linear viscoelastic properties (G' and G'') of the base polymers are shown in Figure 2. As described in the experimental section, different temperatures were selected for the measurement of each polymer (170 °C for PP and 190 °C for PLA) to match the shear stress of each polymer. Key parameters affecting clay dispersion in polymer/clay nanocomposite system are species of clay, viscoelasticity of matrix, and processing conditions. To prove the effect of clay species, we tried to eliminate the effect of viscoelasticity by changing temperature, and processing conditions by fixing mixing rate at 100 rpm. Both polymers show the typical behavior of a polymer melt. The storage (G') and loss (G'') moduli decrease as the angular frequency decreases showing a terminal behavior. The slope of G' and G'' at the terminal region approaches approximately two and one, respectively. Although the moduli for PP and PLA are not exactly same, similar trend of storage and loss modulus for both PP and PLA is observed. In this sense, it can be considered that initial levels of viscoelasticity for neat PP and neat PLA are similar, suggesting that the only meaningful difference in this study is the structural difference or the affinities between the polymer and clay.

The structural development of polymer/clay nanocomposites under an electric field was confirmed by observing G' growth, $[(G'(t) - G'_0)/G'_0]$, during the dynamic time sweep test. Figure 3 shows the G' growth of PP20A with respect to the exposure time under an A.C. electric field with different field strengths (325, 550, 775, and 1000 V/mm). The G' growth of PP20A increases with time under the electric field at lower electric field strength (325, 550 V/mm), whereas the modulus is found to be saturated, as the electric field strength increases (775, 1000 V/mm). The G' after the application of electric field for 20 min

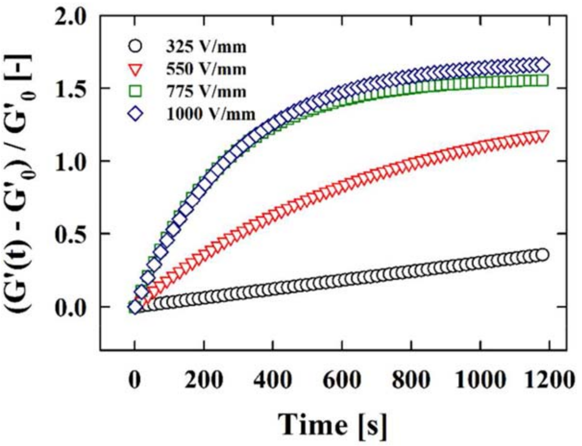

Figure 3. $(G'(t) - G'_0)/G'_0$ of PP20A at 1 rad/s as a function of time at various electric field strengths measured at 170 °C (G'_0 is G' at $t = 0$). [Color figure can be viewed in the online issue, which is available at wileyonlinelibrary.com.]

is highly enhanced with the increase of the field strength. The modulus increment corresponds to the structural development of the nanocomposites due to the application of A.C. field. On the other hand, the G' of PP remains constant without any change even under the electric field (not shown here). Thus, the change in modulus of PP20A can be considered to reflect the structural change of the clay particles. In order to analyze the influence of the A.C. field on the structural development, the modulus change as a function of frequency and the TEM images were analyzed before and after applying the electric field.

The G' of PP20A with various field strengths is given in Figure 4. The G' of pristine PP at 0.1 rad/s is 2.9 Pa, and the terminal slope is approximately 1.5, showing a typical behavior of polymer melts. The G' of PP20A is almost the same with that of neat PP. However, PP20A exhibits a significant increase in G' at

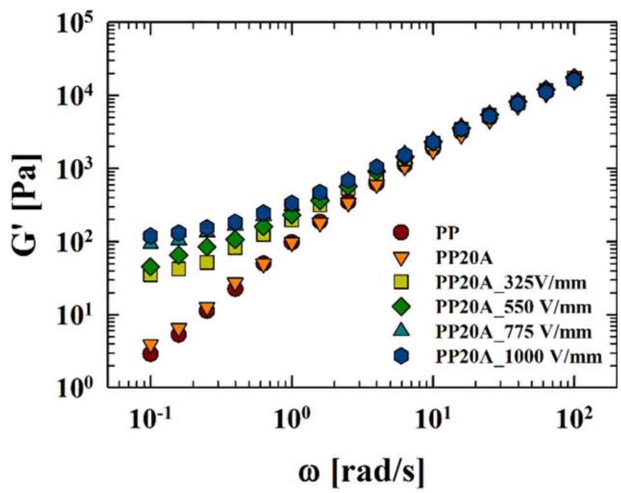

Figure 4. G' of neat PP and PP20A measured after stopping the application of the electric field for 20 min (0, 325, 550, 775, and 1000 V/mm). [Color figure can be viewed in the online issue, which is available at wileyonlinelibrary.com.]

Table III. G' at 0.1 rad/s and the Terminal Slope of PP20A ($E = 1000$ V/mm, $t = 1200$ s)

	0 V/mm	325 V/mm	550 V/mm	775 V/mm	1000 V/mm
G' at 0.1 rad/s	3.92	35.1	45.2	92.9	119
Terminal slope	1.41	0.71	0.62	0.42	0.32

a low frequency (35.1 Pa at 0.1 rad/s) when an electric field of 325 V/mm is applied for 20 min. In addition, the terminal slope decreases to 0.71 at low frequencies. As the intensity of the A.C. field increases, the G' at 0.1 rad/s gradually increases, and the terminal slope decreases (see Table III). The disappearance of this terminal behavior signifies that a networked structure between PP and C20A is formed upon the application of the electric field, which implies an enhancement of clay dispersion.[19,20]

Figure 5 shows the TEM images of PP20A before and after the application of the electric field. Clay tactoids are clearly observed in the PP matrix without an electric field while the tactoids are destroyed and separated layers of silicates are observed when 1000 V/mm is applied. Both the TEM morphology and rheological data confirm that the dispersion of clay particles are enhanced due to the application of the electric field which is in good agreement with previous report.[1–4]

The change in G' of PLA/clay before and after applying the A.C. electric field is shown in Figure 6. Similar to the PP/clay composites, the G' of PLA/clay at the terminal regime increases with the increase in field intensity. For example, the G' of PL30B at 0.1 rad/s is 14.2 Pa and it increases with the increase in field intensity, 34.5 Pa (325 V/mm) < 133 Pa (550 V/mm) < 331 Pa (775 V/mm) < 480 Pa (1000 V/mm). The G' of PL30B increases more than that of PP20A. PL30B contains either thick agglomerates or thin layers of clays before applying the electric field. However, the dispersion is significantly improved after the application of electric field (see Figure 7). The PP/clay composites are basically a micro-composite system consisting of tactoids of clays, whereas PLA/clay composites are intercalated to some degree.[21,22] Because of this difference, the G' of PL30B (Figure 6) is larger than that of PP20A (Figure 4). Additionally, the number of thin layers in PL30B [Figure 7(a)] is much larger than that of PP20A [Figure 5(a)]. The TEM

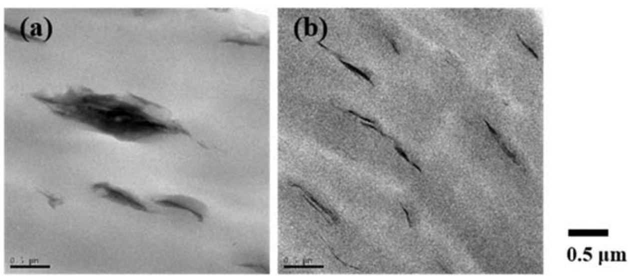

Figure 5. TEM images of PP20A before (a) and after (b) the application of the electric field ($E = 1000$ V/mm, $t = 1200$ s).

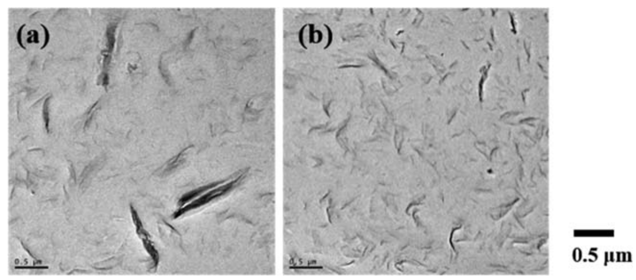

Figure 7. TEM images of PL30B without (a) and with (b) the application of the electric field ($E = 1000$ V/mm, $t = 1200$ s).

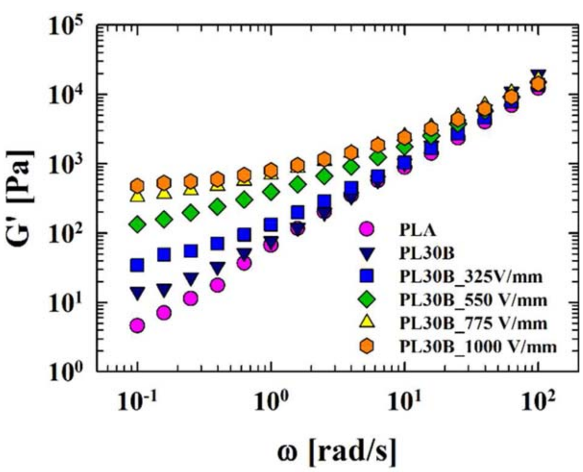

Figure 6. G' of pristine PLA and PL30B measured after stopping the electric field which had been applied for 20 min (325, 550, 775, and 1000 V/mm). [Color figure can be viewed in the online issue, which is available at wileyonlinelibrary.com.]

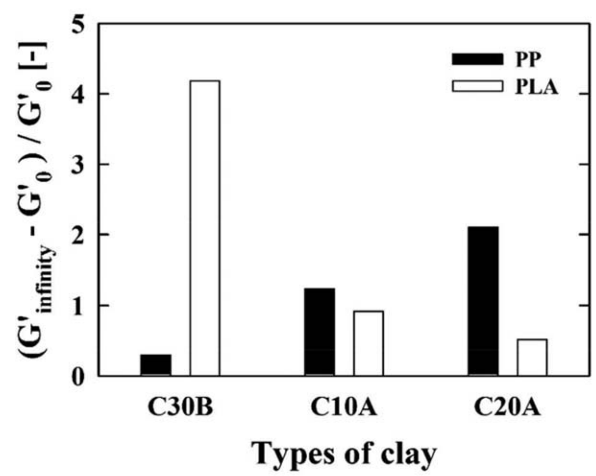

Figure 8. $(G'_{\text{infinity}} - G'_0)/G'_0$ at 1 rad/s measured right after the electric field application (where G'_0 is G' at $t = 0$; G'_{infinity} is G' at $t = 1200$ s under 1 kV/mm).

Table IV. The Parameters Used to get the HSP of the Materials Used in this Study

	Dispersion (δ_d)	Polar interaction (δ_p)	Hydrogen bonding (δ_h)	Total HSP (δ_t)
PP	15.8	0	0	15.8
PLA	15.7	18.4	10.3	26.3
C10A	19.1	2.3	5.5	20.0
C20A	16.9	1.5	5.2	17.7
C30B	21.6	3.2	10.9	24.4

images clearly show enhanced clay dispersion with the electric field, which implies that the A.C. electric field is effective in improving the clay dispersion in both PP/clay and PLA/clay composites (Figures 5 and 7).

Reactivity to Electric Field of Different Composites

The G' growth $[(G'_{\text{infinity}} - G'_0)/G'_0]$ of the PP/clay nanocomposites after the application of the electric field for 20 min at 1 kV was compared with that of the PLA/clay nanocomposites. As shown in Figure 8, the G' growth, $(G'_{\text{infinity}} - G'_0)/G'_0$, of the PP/clay nanocomposites under the electric field increases the most for PP20A followed by PP10A and PP30B. In contrast, the G' of PL30B increases the most followed by PL10A and PL20A. These results demonstrate that C20A and C30B are the most effective combination for PP and PLA, respectively. It also signifies that the A.C. electric field is highly effective for a polymer/clay combination with similar chemical structures. It was previously observed that the gap between the clay platelets was widened and the attraction between clay platelets decreased under the A.C. electric field.[3] Once the gap between the clay galleries widened, the affinity between the polymer and clay had a dominant role in the exfoliation process of the clay.

The solubility parameter is commonly used to estimate the affinity between the chemicals. Especially, the Hansen solubility parameter (HSP) is widely used as a method to predict the affinity between polymers and additives. Thus, the affinities between the polymer and the functional groups of the clays were quantified with the HSP. The total Hansen solubility parameter (δ_t) can be calculated from eq. (1) which consists of three components: the dispersion (δ_d), polar interaction (δ_p), and hydrogen bonding (δ_h) terms. Two materials are more compatible with each other as the difference in the HSP of the two materials becomes smaller. The HSP of the materials used in this study are shown in Table IV.[23,24]

$$\delta_t = \left(\delta_d^2 + \delta_p^2 + \delta_h^2\right)^{\frac{1}{2}} \tag{1}$$

where, $\delta_d = \frac{\left[\sum_z (F_d)_z\right]}{V}$, $\delta_p = \frac{\left[\sum_z (F_p)_z^2\right]^{\frac{1}{2}}}{V}$, and $\delta_h = \left(\sum_z \text{-} U_z / V\right)^{\frac{1}{2}}$.

Here, F is the attraction constant, U is the internal energy, and V is the Van der Waals volume. The G' growth under a 1 kV electric field for 20 min $[(G'_{\text{infinity}} - G'_0)/G'_0]$ with the HSP difference ($\Delta\delta = |\delta_{\text{polymer}} - \delta_{\text{clay}}|$) is shown in Figure 9. The G' growth is inversely proportional to the HSP difference, irrespective of polymer species and electric field strength. Additionally, the G' growth becomes larger with the increase in electric field strength. According to the HSP calculation, PP has the highest affinity with C20A followed by C10A and C30B. On the other hand, the preferential clay of PLA is C30B followed by C10A and C20A. The non-polar PP has the highest affinity with C20A which also has the non-polar functional groups, while a polar PLA is the most compatible with C30B which has polar functional groups (Table I). These results are in good agreement with the different reactivities to the electric field of the polymer/clay nanocomposites as shown in Figure 8. This suggests that the A.C. electric field for clay exfoliation is more efficient for polymer/clay combinations with higher affinities. The affinity between the polymer and the clay is one of the most important factors when fabricating polymer/clay nanocomposites by applying the electric field.

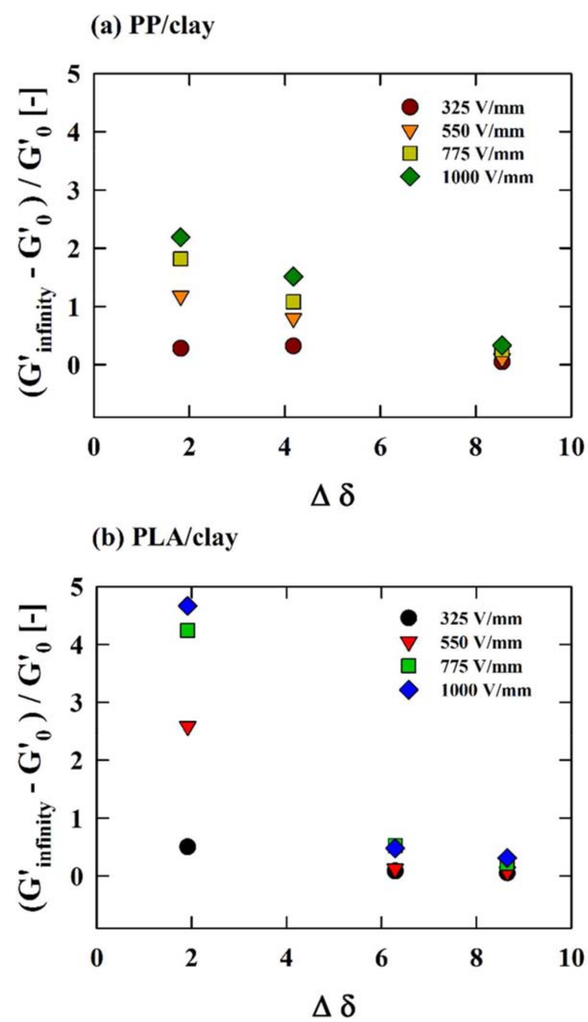

Figure 9. $(G'_{\text{infinity}} - G'_0)/G'_0$ versus $\Delta\delta$ ($|\delta_{\text{polymer}} - \delta_{\text{clay}}|$) for (a) PP/clay and (b) PLA/clay nanocomposites after the application of the electric field ($E = 325$, 550, 775, and 1000 V/mm; $t = 1200$ s). [Color figure can be viewed in the online issue, which is available at wileyonlinelibrary.com.]

CONCLUSIONS

Polymer/clay nanocomposites with two base polymers (non-polar PP and polar PLA) and three kinds of organoclays functionalized with different surfactants (Cloisite 10A, Cloisite 20A, and Cloisite 30B) were melt compounded, and the efficiency of the electric field was investigated in PP/clay and PLA/clay nanocomposites. The dynamic moduli of the composites increased under the A.C. field, and the terminal behavior disappeared. The G' growth as well as the disappearance of the terminal behavior in the low frequency domain suggested the formation of a network structure of the PP/clay and PLA/clay nanocomposites under an A.C. electric field. Rheological and morphological analyses revealed that the A.C. electric field improved the dispersion state of the organoclays. The A.C. electric field was more effective for the PLA/clay composites than for the PP/clay composites. The electric field efficiency of three different types of clays for PP showed opposite trend compared with PLA. These results implied that the response to the electric field was different according to the affinities between the polymers and clays. To analyze the influence of affinities, we quantified the affinities between the polymers and clays by the Hansen solubility parameter. The electric field was the most effective for the polymer/clay combinations of PP/Cloisite 20A and PLA/Cloisite 30B which had the highest affinities to each other.

ACKNOWLEDGMENTS

This work was supported by the Korea Institute of Energy Technology Evaluation and Planning (KETEP) and the Ministry of Trade, Industry & Energy (MOTIE) of the Republic of Korea (No. 20141010101880).

REFERENCES

1. Kim, D. H.; Park, J. U.; Ahn, K. H.; Lee, S. *J. Macromol. Rapid. Commun.* **2003**, *24*, 388.
2. Park, J. U.; Choi, Y. S.; Cho, K. S.; Kim, D. H.; Ahn, K. H.; Lee, S. J. *Polymer* **2006**, *47*, 5145.
3. Kim, D. H.; Cho, K. S.; Mitsumata, T.; Ahn, K. H.; Lee, S. J. *Polymer* **2006**, *47*, 5938.
4. Kim, D. H.; Park, J. U.; Cho, K. S.; Ahn, K. H.; Lee, S. J. *Macromol. Mater. Eng.* **2006**, *291*, 1127.
5. Bharadwaj, R. K. *Macromolecules* **2001**, *34*, 9189.
6. Liu, H.; Lim, H. T.; Ahn, K. H.; Lee, S. J. *J. Appl. Polym. Sci.* **2006**, *104*, 4024.
7. Hong, J. S.; Kim, Y. K.; Ahn, K. H.; Lee, S. J. *J. Appl. Polym. Sci.* **2007**, *108*, 565.
8. Kim, D. H.; Fasulo, P. D.; Rodgers, W. R.; Paul, D. R. *Polymer* **2008**, *49*, 2492.
9. Kiliaris, P.; Papaspyrides, C. D. *Prog. Polym. Sci.* **2010**, *35*, 902.
10. Cho, S.; Hong, J. S.; Lee, S. J.; Ahn, K. H.; Covas, J. A.; Maia, J. M. *Macromol. Mater. Eng.* **2010**, *296*, 341.
11. Jang, K.; Lee, J. W.; Hong, I.-K.; Lee, S. *Korea-Aust. Rheol. J.* **2013**, *25*, 145.
12. Cai, D.; Song, M. *J. Appl. Polym. Sci.* **2015**, *132*, 41314.
13. Ock, H. G.; Kim, D. H.; Ahn, K. H.; Lee, S. J.; Maia, J. M. *Eur. Polym. J.* **2016**, *76*, 216.
14. Sun, T.; Garcés, J. M. *Adv. Mater.* **2002**, *14*, 128.
15. Nguyen, Q. T.; Baird, D. G. *Adv. Polym. Technol.* **2006**, *25*, 270.
16. LeBaron, P. C.; Wang, Z.; Pinnavaia, T. *J. Appl. Clay Sci.* **1999**, *15*, 11.
17. Singla, P.; Mehta, R.; Upadhyay, S. N. *Appl. Clay Sci.* **2014**, *95*, 67.
18. Matrínez-Colunga, J. G.; Sánchez-Valdés, S.; Ramos-deValle, L. F.; Muñoz-Jiménez, L.; Ramírez-Vargas, E.; Ibarra-Alonso, M. C.; Lozano-Ramirez, T.; Lafleur, P. G. *J. Appl. Polym. Sci.* **2014**, *131*, 40631.
19. Solomon, M. J.; Almusallam, A. S.; Seefeldt, K. F.; Somwangthanaroj, A.; Varadan, P. *Macromolecules* **2001**, *34*, 1864.
20. Durmus, A.; Kasgoz, A.; Macosko, C. W. *Polymer* **2007**, *48*, 4492.
21. Krikorian, V.; Pochan, D. *J. Chem. Mater.* **2003**, *15*, 4317.
22. Ray, S. S.; Okamoto, M. *Prog. Polym. Sci.* **2003**, *28*, 1539.
23. Barton, A. F. M. Handbook of Solubility Parameters and Other Cohesion Parameters, 2nd ed.; CRC Press: Florida, **1991**; Chapter 14.
24. Hansen, C. M. Hansen Solubility Parameters: A User's Handbook, 2nd ed.; CRC Press: Florida, **2007**; Chapter 2.